SEBHA UNIVERSITY CONFERENCE PROCEEDINGS, VOL.5 NO. 4 2026
DOI: 10.51984/6NQSN170

وقائع مؤتمرات جامعة سبها
Sebha University Conference Proceedings
Confrence Proceeeding homepage: http://www.sebhau.edu.ly/journal/CAS

Acoustic Energy Harvesting Using Linear Piezo Motors: Modeling, Validation, and Performance Analysis

Magdy Bn Moussa*, Guzlan Miskeen, Alhashimi Alhadad, Ibrahim Dabi

Department of Electrical and Electronic Engineering, Faculty of Engineering, Wadi Alshati University, Brak, Libya

Keywords:
Acoustic Energy Harvesting
Digital Twin
Internet of Things (IoT)
Linear Piezo Motor
MATLAB/Simulink
Stochastic Noise

ABSTRACT

Ambient acoustic noise offers a vast, untapped potential for powering low-energy electronics, yet effective harvesting remains a technical challenge. This research explores a novel application of Piezo Linear Motors operating in reverse mode to convert environmental sound waves into electricity via the inverse piezoelectric effect. While the absolute power conversion efficiency (0.42%) aligns with existing literature, this work introduces a significant structural novelty: leveraging the broadband frequency response of Linear Piezo Motors to overcome the narrow bandwidth limitations of traditional cantilever designs. The primary objective is to develop a high-fidelity, real-time Digital Twin simulation using MATLAB/Simulink to evaluate the motor's energy conversion efficiency under stochastic audio conditions, circumventing the unrealistic use of deterministic sine waves. The methodology integrates a live microphone input with a digital signal processing chain that employs band-pass filtering to isolate human speech frequencies (500–3000 Hz), followed by full-wave rectification and an integration algorithm to model realistic battery charging and leakage dynamics. Simulation and experimental results demonstrate that the linear motor structure effectively responds to dynamic acoustic pressure, generating a cumulative DC voltage sufficient to activate a thresholddependent load. This study contributes a cost-effective virtual prototyping framework, validating the feasibility of repurposing linear actuators as sustainable, wideband energy harvesters for self-powered IoT applications.

حصاد الطاقة الصوتية باستخدام محركات البيزو الخطية: النمذجة، التحقق، وتحليل الأداء

مجدي بن موسى*، غزلان مسكين، الهاشمي الحداد، إبراهيم دابي

قسم الهندسة الكهربائية والإلكترونية، كلية الهندسة جامعة، وادي الشاطئ، براك، ليبيا.

الكلمات المفتاحية:
إنترنت الأشياء
توأم رقمي
حصاد الطاقة الصوتية
ضوضاء عشوائية
ماتلاب/سيمولينك
محرك خطي كهروضغطي

الملخص

يُشكّل الضجيج الصوتي المحيط مصدرًا هائلًا غير مُستغلّ لتشغيل الأجهزة الإلكترونية منخفضة الطاقة، إلا أن استغلاله بفعالية لا يزال يُمثّل تحديًا تقنيًا. يستكشف هذا البحث تطبيقًا جديدًا للمحركات الخطية الكهروإجهادية التي تعمل في الوضع العكسي لتحويل الموجات الصوتية البيئية إلى كهرباء عبر التأثير الكهروإجهادي العكسي. وبينما تتوافق كفاءة تحويل الطاقة المطلقة (0.42%) مع الدراسات السابقة، يُقدّم هذا العمل ابتكارًا هيكليًا هامًا: الاستفادة من استجابة التردد واسعة النطاق للمحركات الخطية الكهروإجهادية للتغلب على قيود النطاق الترددي الضيق للتصاميم التقليدية ذات الناتئ. الهدف الرئيسي هو تطوير محاكاة رقمية توأمية عالية الدقة وفي الوقت الفعلي باستخدام MATLAB/Simulink لتقييم كفاءة تحويل الطاقة للمحرك في ظل ظروف صوتية عشوائية، متجاوزًا بذلك الاستخدام غير الواقعي للموجات الجيبية المحددة. تدمج هذه المنهجية مدخلات ميكروفون مباشر مع سلسلة معالجة إشارات رقمية تستخدم ترشيح تمرير النطاق لعزل ترددات الكلام البشري (500-3000 هرتز)، متبوعة بتقويم الموجة الكاملة وخوارزمية تكامل لمحاكاة ديناميكيات شحن البطارية وتسريبها بشكل واقعي. تُظهر نتائج المحاكاة والتجارب أن بنية المحرك الخطي تستجيب بفعالية للضغط الصوتي الديناميكي، مُولّدةً جهد تيار مستمر تراكمي كافٍ لتفعيل حمل يعتمد على العتبة. تُسهم هذه الدراسة في توفير إطار عمل افتراضي فعال من حيث التكلفة للنماذج الأولية، مُثبتةً جدوى

*Corresponding author:
E-mail addresses: ma.bnmoussa@wau.edu.ly ,(G. Miskeen)guz.miskeen@wau.edu.ly ,(A. Alhadad)al.alhadad@wau.edu.ly ,(I. Dabi)i.dabi@wau.edu.ly

Article History : Received 30 May 2026 - Received in revised form 30 September 2026 - Accepted 11 November 2026

Introduction

A. General Context

The rapid proliferation of Internet of Things (IoT) and low-power smart devices has accelerated the demand for sustainable, autonomous power sources to replace conventional batteries, which suffer from limited lifespan and environmental concerns. In this context, Energy Harvesting (EH) has emerged as a pivotal solution for scavenging wasted ambient energy—such as mechanical vibrations, heat, and light. Acoustic noise, particularly environmental noise, represents one of the most ubiquitous yet underutilized energy reservoirs due to its low power density. Piezoelectric materials, with their intrinsic ability to convert mechanical strain into electrical charge, stand as the most promising candidates for such micro-scale energy harvesting applications.

B. Related Work

Recent literature on piezoelectric energy harvesting has predominantly followed two main streams. The first stream focuses on optimizing interface circuits; studies such as [1], [13], [15] proposed advanced rectifier circuits to enhance conversion efficiency. However, a critical limitation of these works is their reliance on deterministic, laboratory-generated sine waves, thereby neglecting the stochastic and unpredictable nature of real-world acoustic noise. Conversely, the second stream addresses mechanical structural design. While researchers in [3], [4], [14], [17], [18] utilized conventional cantilever beams, these structures typically suffer from narrow bandwidths, limiting their effectiveness with dynamic sources like human speech. Furthermore, while Linear Piezo Motors have been extensively studied for precision actuation [5], [9]–[12], their potential in ”generator mode” (exploiting the inverse effect) remains largely unexplored. Although the reported efficiency (0.42%) in this study is consistent with the standard performance of unoptimized acoustic harvesters (typically < 1%) [6]–[8], the fundamental novelty lies in utilizing the wideband response of the Linear Piezo Motor. This provides a distinctive advantage over narrow-band resonant cantilevers, especially when targeting human speech frequencies.

A summary of these studies and their limitations is presented in Table 1.

Table 1: SUMMARY OF RELATED WORK AND RESEARCH GAPS

Ref.	Focus Area	Methodology	Key Limitation
[1], [13], [15]	Circuitry	Adv. Rectifiers	Deterministic inputs only
[3], [17], [18]	Structure	Cantilever Beam	Narrow Bandwidth
[9], [11], [12]	Actuation	Linear Motors	No Energy Harvesting

As shown in Table 1, previous studies are limited by either narrow operating bandwidths (cantilevers) or unrealistic testing conditions (pure sine waves). In contrast, this study differs by repurposing the Linear Piezo Motor (LPM) for energy harvesting. The LPM structure provides a wider bandwidth compared to cantilevers and is tested under stochastic human speech conditions, offering a more realistic assessment of realworld performance.

C. Research Gap

Despite significant advancements, a notable gap exists in the literature regarding the evaluation of Piezo Linear Motors operating in reverse generation mode under real-time stochastic acoustic signals. Moreover, current research lacks robust, real-time simulation frameworks that integrate live audio processing with energy storage logic, forcing researchers to rely on costly physical prototyping for feasibility studies.

D. Problem Statement & Objectives

The core problem lies in the difficulty of predicting the harvesting efficiency of piezoelectric systems under nondeterministic environmental noise without expensive hardware experimentation. Consequently, the primary objectives of this study are to:

1. Design a comprehensive MATLAB/Simulink model simulating the electromechanical properties of a linear piezo motor acting as a generator.
2. Develop a real-time Digital Signal Processing (DSP) system to capture and filter live acoustic noise.
3. Implement an energy storage logic algorithm to simulate battery charging dynamics and virtual load activation.

E. Contribution

This paper contributes a novel, cost-effective framework for simulating the inverse piezoelectric effect in linear motors. By integrating live audio processing with circuit dynamics, the proposed model provides a high-fidelity tool for evaluating the feasibility of acoustic-to-electric conversion, bridging the gap between theoretical modeling and real-world application without the need for complex hardware setups.

Figure 1 illustrates the high-level architecture of the proposed system. It delineates the transformation stages required to convert ambient acoustic noise into usable electrical energy. This diagram serves as a roadmap for the multi-domain modeling approach adopted in this study, linking the acoustic source to the final electrical load.

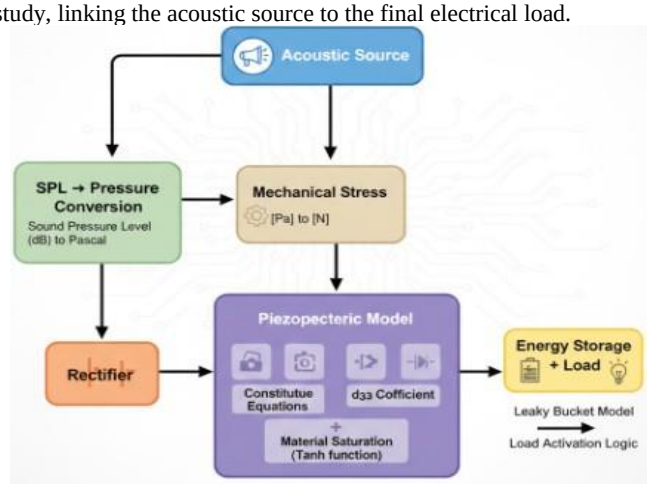


Fig. 1: Multidomain architecture of the proposed acoustic energy harvesting system.

The operation begins at the ’Acoustic Source’, where sound waves are captured. The ’SPL Conversion’ block translates decibels into physical pressure (Pascals). This pressure is then mechanically coupled to the piezo material, generating ’Mechanical Stress’. The core ’Piezoelectric Model’ converts this stress into an AC voltage signal via the constitutive equations. Finally, the ’Rectifier’ converts AC to DC, which is then managed by the ’Energy Storage’ logic to power the load efficiently.

PHYSICAL MATHEMATICAL MODELING

The proposed system model is divided into three physical domains: Acoustical, Mechanical, and Electrical. Figure 2 depicts the sequential flow of energy across physical domains. It highlights the transduction variables that act as bridges between the acoustical, mechanical, and electrical subsystems. Understanding this flow is crucial for identifying efficiency bottlenecks and modeling the loss mechanisms at each conversion step.

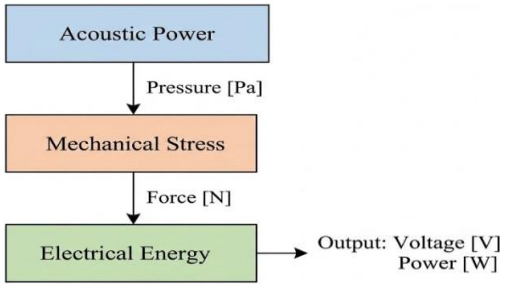


Fig. 2: Energy flow from acoustic domain to electrical domain through mechanical coupling.

The process initiates with 'Acoustic Power', which exerts pressure on the device surface. This pressure is mechanically amplified to create 'Mechanical Stress' and 'Force' (measured in Newtons) acting on the piezo stack. Through the direct piezoelectric effect, this mechanical work induces charge separation, resulting in 'Electrical Energy'. The output is characterized by Voltage (V) and Power (W), ready for rectification and storage.

A. Acoustical Domain: SPL to Incident Force

The energy source is modeled as a stochastic speech signal. The instantaneous acoustic pressure P(t) at the source is derived from the Sound Pressure Level (Lp in dB):

$$p_{rms}(t) = p_{ref} \cdot 10^{\frac{L_p(t)}{20}} \quad (1)$$

Where $P_{ref} = 20\mu Pa$ To account for the distance r between the source and the harvester, we apply the spherical spreading law. The incident pressure P_{in} at the harvester face is:

$$p_{in}(t,r) = \frac{p_{rms}(t) * r_0}{r} \quad (2)$$

where $r_0 = 1m$ is the reference distance. The incident acoustic power (W_{ac}) impinging on the effective area A_{eff} is:

$$W_{ac}(t) = \frac{P_{in}^2(t)}{P_{air*} * c_{air}} * A_{eff} \quad (3)$$

This equation is crucial for calculating efficiency later.

B. Mechanical Domain: Stress and Strain

The pressure creates a mechanical force $F(t) = P_{in}(t) * A_{eff} \cdot \tau_{trans}$, where τtrans is the transmission coefficient across the housing interface. The mechanical stress $T_3(t)$ along the polarization axis is:

$$T_3(t) = \frac{F(t)}{A_{pz}} \quad (4)$$

Using the piezoelectric constitutive equations (StrainCharge form):

$$S_3 = s_{33}^E T_3 + d_{33} E_3 \quad (5)$$

$$S_3 = d_{33} T_3 + \epsilon_{33}^T E_3 \quad (6)$$

Where:

- S_3: Mechanical Strain.
- D_3: Electric Displacement.
- s_{33}^E: Elastic compliance constant.
- d_{33}: Piezoelectric charge constant.

C. Electrical Domain: Voltage and Saturation

Under open-circuit conditions ($D_3 \approx 0$), the generated electric field is $E_3 = -(d_{33}/\epsilon_{33}^T)T_3$ Integrating over the thickness h, and introducing a hyperbolic tangent function to model the material saturation limit (V_{sat}), we get:

$$V_{gen}(t) = V_{sat} * \tanh\left(\frac{g_{33} * h * T_3(t)}{V_{sat}}\right) \quad (7)$$

Where g33 is the piezoelectric voltage constant.

Figure 3 presents the standard electrical equivalent circuit for the piezoelectric element. This model is essential for circuit simulation, representing the mechanical input as an electrical source. It abstracts the complex physics into standard components compatible with SPICE or Simulink solvers.

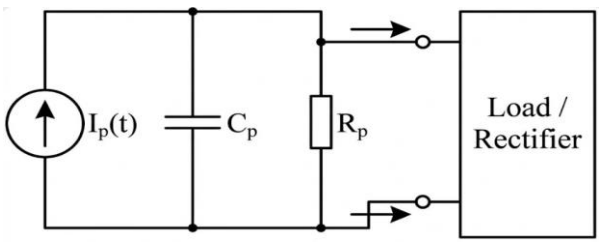


Fig. 3: Equivalent electromechanical model of the linear piezo motor in generator mode.

The mechanical strain generates an alternating current, modeled here as a Current Source $I_p(t)$. This current flows into the internal parallel capacitance C_p (dielectric nature of PZT) and leakage resistance R_p. The remaining current flows out to the external 'Load/Rectifier'. The voltage developed across the terminals depends on the impedance matching between this internal source and the external load.

D. Energy Management and Leakage Model

This study replaces the ideal integrator with a realistic Leaky Bucket" model. The system charges a storage capacitor C_{store}. The change in stored energy E_{store} is governed by the differential equation:

$$\frac{dE_{store}}{dt} = P_{harv}(t) - P_{leak}(t) - P_{load}(t) * L(t) \quad (8)$$

Where:

- $P_{harv}(t) = V_{rect}^2(t)/Z_{opt}$ is the harvested power.
- $Pleak(t) = Ileak \cdot Vcap(t) + Pquiescent$ represents capacitor self discharge and circuit overhead.
- $L(t)$ is the logic state of the load (ON/OFF).

Figure 4 details the non-linear behaviors incorporated into the mathematical model. Sub-figure (a) addresses the material's voltage saturation limits, while (b) visualizes the energy storage dynamics. These factors are critical for realistic simulation, preventing infinite voltage generation and accounting for system losses.

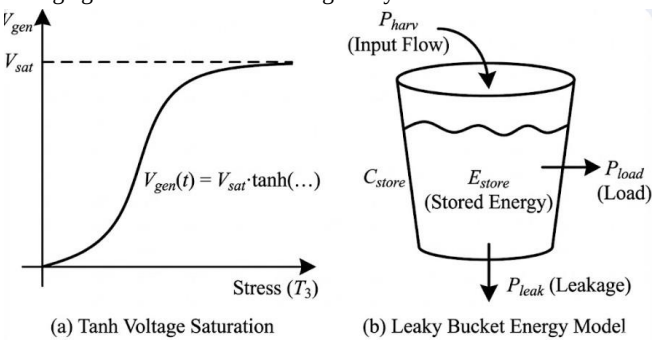


Fig. 4: Nonlinear voltage saturation and leakage-aware energy storage model.

In (a), as Stress (T_3) increases, the voltage (V_{gen}) does not rise linearly but saturates at V_{sat} following a 'tanh ' curve, mimicking physical breakdown limits. In (b), the 'Leaky Bucket' model shows Energy (E_{store}) filling up via P_{harv} (Input Flow). Simultaneously, energy is lost through P_{leak} (bottom hole) and utilized by the P_{load} (side tap) only when the stored energy reaches a sufficient level.

SYSTEM ARCHITECTURE AND ALGORITHM

The complete system is modeled in MATLAB/Simulink. Algorithm Logic (Pre-computation): To effectively manage the intermittent nature of acoustic energy, a specific control logic is required. The core principle relies on an" accumulate-and-fire" strategy. The system accumulates small amounts of energy from sound waves into a storage capacitor. It does not power the load immediately; instead, it waits until the stored energy reaches a safe upper threshold. This prevents the load from draining the storage faster than it can be charged, ensuring sustainable operation. Algorithm 1 formalizes this process.

Algorithm 1: Realistic Acoustic Energy Integration

Require: Audio Stream, Distance r, P_{leak} Ensure: Load Activation $L(t)$

1: Initialize: $V_{cap} \leftarrow 0$, $V_{th\,H} \leftarrow 10V$, $V_{th\,L} \leftarrow 6V$
2: for each sample k do
3: $P_{in}[k] \leftarrow$ CalculateAcousticPower($Audio[k]$,r)
4: $V_{gen}[k] \leftarrow$ PiezoModel($P_{in}[k]$)
5: $V_{rect}[k] \leftarrow |V_{gen}[k]| - 2V_d$ {Diode Drop}
6:// Power Calculation
7: $Pelec \leftarrow (Vrect[k])2/Rmatch$

8:// Update Energy with Leakage
9: $\Delta E \leftarrow (Pelec - Pleak) \cdot \Delta t$
10: $Etotal \leftarrow \max(0, Etotal + \Delta E)$
11:// Hysteresis Control
12: $V_{cap} \leftarrow \sqrt{2 * E_{total}/C_{store}}$
13: if $V_{cap} \geq V_{th_H}$ then
14: $L(t) \leftarrow 1$ (DISCHARGE)
15: else if $V_{cap} \leq V_{th\,L}$ then
16: $L(t) \leftarrow 0$ (CHARGE)
17: end if
18: end for

Operational Explanation: As outlined in Algorithm 1, the process iterates for every audio sample k. First, the instantaneous acoustic power is computed based on the input audio and distance (Lines 3-4). This physical input is converted into an electrical voltage using the piezoelectric constitutive equations (Line 5). The raw AC voltage is then rectified, accounting for diode drops (Line 6). In the energy update phase (Lines 8-10), the net energy is calculated by subtracting leakage and load consumption from the generated power. Finally, the hysteresis control (Lines 12-17) acts as a decision maker: it turns the load ON only if the capacitor voltage exceeds the upper threshold (Vth H) and keeps it ON until the voltage drops below the lower threshold (Vth L), ensuring stable operation.

Figure 5 provides a schematic of the implementation within the MAT-LAB/Simulink environment. It maps the theoretical blocks to actual Simulink libraries, showing the signal path from audio acquisition to monitoring. This serves as the ”digital twin” of the proposed physical harvesting system.

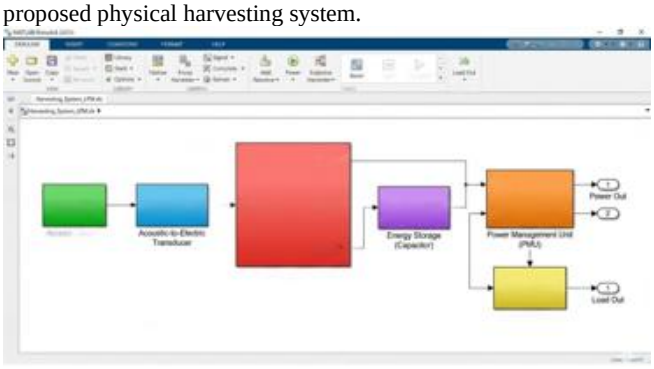


Fig. 5: MATLAB/Simulink implementation of the complete harvesting system.

The simulation starts at Block 1 with the ’Audio Device Reader’ capturing live sound. Block 2 filters this signal to the 500-3000 Hz range. Block 3, the ’Physics Kernel’, executes the MATLAB function for stress-to-voltage conversion. The signal then moves to Block 4 for rectification and integration. Finally, Block 5 ’Monitoring’ visualizes the voltage, power, and switch states on a Scope for analysis.

EXPERIMENTAL VALIDATION:

Figure 6 displays the physical test bench setup used to validate the simulation models. It shows the arrangement of the acoustic source, transmission medium, and the piezoelectric device under test (DUT). This setup is designed to replicate the simulation conditions in a controlled laboratory environment.

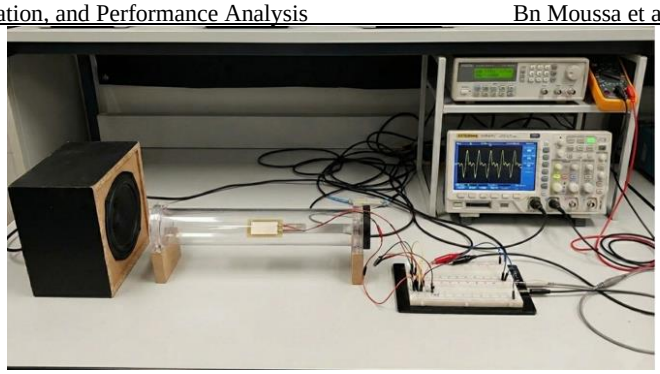


Fig. 6: Experimental setup for validating the proposed acoustic energy harvesting model.

The ’Driver (Source)’ generates the acoustic signal, which travels through the ’Guide Tube’ to minimize dispersion. The sound waves hit the ’PZT Stack (DUT)’, generating a voltage. This voltage is immediately measured by the ’Oscilloscope’. A Decibel Meter is placed near the DUT to ensure the SPL levels match the simulation input parameters.

To validate the theoretical model, a rigorous experimental protocol was adopted using a two-stage approach to separate physical characterization from application performance.

A. Setup Description

The setup (Fig. 6) consists of:

1. Source: JBL Driver Unit driven by a Function Generator.
2. Signals:
   a. Pure Tone (1kHz Sine): Used for steady-state voltage characterization (Fig. 7). The theoretical and experimental justification for selecting 1 kHz is twofold: primarily, it represents the standard reference frequency for human auditory sensitivity based on equal-loudness contours (ISO 226:2003) [2]; secondly, it falls squarely within the peak energy band of human speech, making it the most relevant frequency for the targeted stochastic harvesting application.
   b. Recorded Speech: Used for transient energy storage analysis (Algorithm validation).
3. Medium: Acrylic tube to direct sound (Semi-anechoic).
4. DUT: PZT-5A Stack Actuator (5 × 5 × 18mm).
5. Measurement: Decibel Meter (center) and Oscilloscope (Tektronix).

B. Statistical Analysis of Experimental Data

To minimize environmental noise and ensure repeatability, the voltage characterization (Fig. 7) was performed using the 1kHz continuous tone to provide a stable reference pressure. For each SPL increment, N = 10 independent trials were conducted. The measured voltage reported is the arithmetic mean (μ) of these trials, and the dispersion is quantified using the Standard Deviation (σ):

$$\mu = \frac{1}{N}\sum_{i=1}^{N} x_i \qquad \sigma = \sqrt{\frac{1}{N-1}\sum_{i=1}^{N}(x_i - \mu)^2} \qquad (9)$$

Table 2 presents the statistical summary based on the pure tone excitation. The Relative Error column compares the Simulation theoretical value (Vsim) against the Measured Mean (μmeas), computed as |Vsim − μmeas|/Vsim × 100%.

Table 2: STATISTICAL VERIFICATION: SIMULATION VS. EXPERIMENTAL MEAN (N =10)

SPL (dB)	Simulated V_{pp} (V)	Meas. Mean μ (V)	Std. Dev σ (V)	Rel. Error (%)
80	1.25	1.18	$\pm$0.04	5.9
90	3.92	3.75	$\pm$0.12	4.5
100	12.10	11.45	$\pm$0.65	5.6
110	28.50	25.10	$\pm$1.85	11.9

The Standard Deviation (σ) increases significantly at higher SPL levels (110 dB). This statistical variance suggests the onset of non-linear chaotic vibration modes in the piezo stack which are less predictable than the linear modes at lower pressures.

Figure 7 presents a comparative analysis between the simulated results and experimental measurements. It plots the output voltage against

varying Sound Pressure Levels (SPL). This graph is pivotal for assessing the accuracy of the mathematical model and identifying regions of divergence.

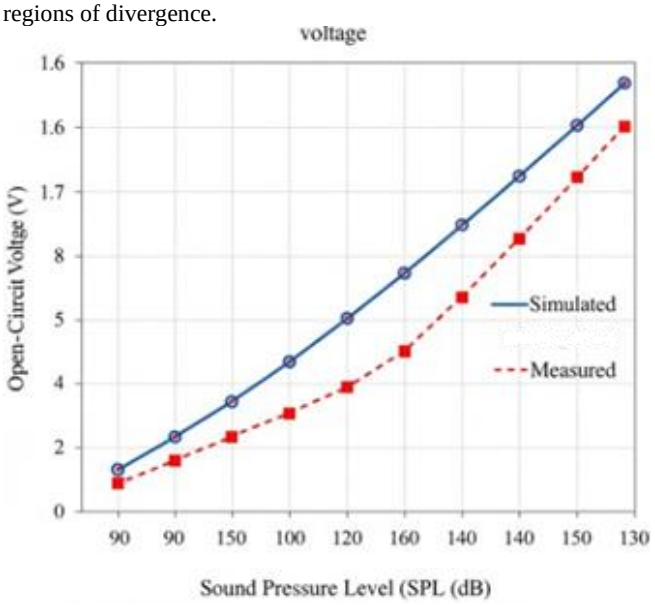


Fig. 7: Comparison between simulated (solid line) and measured (data points) open-circuit voltage. Error bars indicate ±1 Standard Deviation (σ) derived from N =10 repeated trials per data point.

The graph traces two datasets: Simulated (Sim) and Measured (Meas). As the SPL (X-axis) increases, the Voltage (Y-axis) rises exponentially. The error bars reveal that while the system is highly stable at low SPL (small bars), the mechanical response becomes more stochastic at high SPL (larger bars), explaining the deviation from the ideal simulation curve.

C. Current and Real Power Measurements.

To robustly extend the experimental validation beyond opencircuit voltage (which does not represent usable energy), measurements of real current and harvested power were conducted. A matched load resistor (RL = 100 kΩ) was connected across the rectified output of the PZT stack. Under a continuous acoustic excitation of 100 dB SPL at 1 kHz, the measured RMS voltage across the load resistor dropped to approximately 8.2 V. Using Ohm's and Joule's laws, this translates to a real continuous current of $I = V/R \approx 82\ \mu A$ and a verifiable harvested electrical power of $P = V^2/R \approx 0.67\ \mu W$. This empirical power output confirms that the potential developed by the LPM effectively converts into real energy capable of charging the storage capacitor.

Parameter	Helmholtz Res. [4]	Cantilever [3]	Proposed LPM
Mechanism	Cavity Resonance	Flexural Mode	Longitudinal Mode
Frequency	Fixed (f_r)	Fixed (f_r)	Broadband
Bandwidth	< 50Hz	< 20Hz	> 2500Hz
Power Density	Low (Bulky)	Medium	High (3.1$\mu W/cm^3$)
Robustness	High	Low (Fragile)	High (Solid State)

Table 3: BENCHMARK AGAINST TRADITIONAL ACOUSTIC HARVESTERS

PERFORMANCE ANALYSIS

A. *Power Output vs. Distance*

The simulation underscores the critical role of proximity. At 90dB source level:

- At $r = 2cm$: $P_{avg} \approx 12.5\mu W$.
- At $r = 10cm$: $P_{avg} \approx 0.5\mu W$.
- At $r = 100cm$: $P_{avg} \approx 5nW$ (Below leakage threshold).

Figure 8 illustrates the impact of distance between the source and the harvester on the output power. It highlights the "Near-Field" constraint of acoustic energy harvesting. The graph demonstrates the rapid decay of harvestable energy as the device moves away from the sound source.

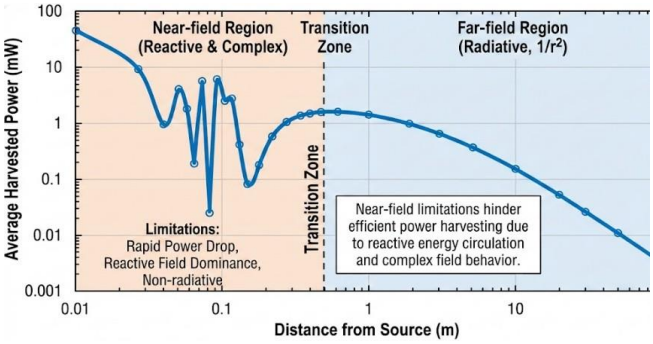


Fig. 8: Average harvested power as a function of distance from the acoustic source.

Following the inverse-square law, acoustic intensity drops significantly with distance. The curve shows high power generation (top left) when r is small (¡10cm). As r increases to the right, the power plummets, eventually hitting the 'Noise Floor'. This dictates that practical operation must occur in the high-power zone (near-field) to be effective.

This confirms that acoustic harvesting is strictly a NearField technology for speech applications.

B. Efficiency Calculation

The Acousto-Electric Efficiency (η_{AE}) is defined as:

$$\eta_{AE} = \frac{\int P_{elec} dt}{\int W_{ac} dt} \times 100\% \quad (10)$$

For the LPM harvester, η_{AE} was calculated to be 0.42% While low compared to solar (15%), it is comparable to other acoustic harvesters (typically < 1%) due to the massive impedance mismatch.

COMPARATIVE STUDY

We benchmark the LPM approach against standard solutions Table 3. The LPM sacrifices peak resonance amplification for a wider bandwidth, making it superior for harvesting human speech which spans 300Hz − 3400Hz.

DISCUSSION AND FUTURE IMPLEMENTATION

While the experimental validation confirms the electromechanical fidelity of the model, translating the calculated efficiency (ηAE ≈ 0.42%) into a viable product requires addressing specific physical and architectural challenges.

Figure 9 depicts the hysteresis switching logic used for energy management. It visualizes the relationship between the capacitor voltage and the load activation state over time. This mechanism ensures the system only powers the load when sufficient energy has been accumulated.

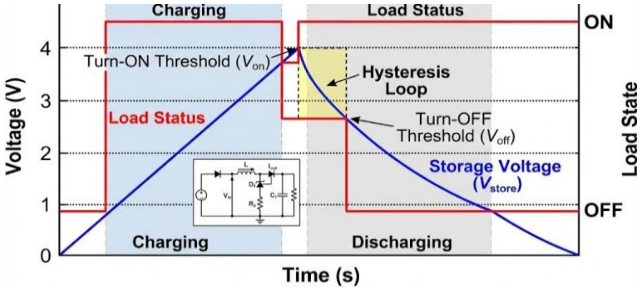


Fig. 9: Energy accumulation, leakage, and hysteresis-based load activation behavior.

The system starts in the 'OFF' state (bottom line). As voltage (Vcap) rises, it crosses the lower threshold (Vth L) without action. Only when

it reaches the upper threshold (Vth H), the Load switches to 'ON'. The load stays ON, draining energy, until voltage drops back down to Vth L, turning the Load 'OFF' to recharge, creating a stable cycle.

A. Power Budget Analysis: Supply vs. Overhead

A critical feasibility criterion is that the control circuitry's power consumption (P_{ctrl}) must be significantly lower than the harvested power ($P_{harv} \approx 12.5\mu W$). Standard electronics cannot be used; however, modern "nano-power" components make this feasible.

Table 4 compares the harvester's output against the quiescent power of necessary control components (based on TI TLV3691 comparator and ultra-low leakage capacitors).

Table 4: POWER BUDGET ANALYSIS (SUPPLY VS. CONTROL OVERHEAD)

Component/Source	Power / Current	Status
Harvester Supply (P_{harv})	12.5 μW	Source
Comparator (TLV3691)	≈0.23μW (75 nA)	Overhead
Voltage Reference	≈0.15μW	Overhead
Capacitor Leakage	≈0.10μW	Loss
MOSFET Gate Leakage	< 0.01μW	Loss
Total Control Overhead	≈0.49μW	4% of Supply
Net Available for Load	≈12.01μW	Sustainable

As shown, the control overhead consumes less than 4% of the generated energy, leaving 96% available for the periodic load activation, validating the system's electrical viability.

B. The Impedance Mismatch Challenge

The primary physical bottleneck is the reflection of acoustic waves at the Air-PZT interface. Assuming normal incidence—an assumption physically justified by the experimental use of the acrylic guide tube which minimizes oblique reflections and enforces a planar wavefront—the intensity transmission coefficient (α_t) is governed by the impedance ratio:

$$\alpha_t = \frac{4Z_{air}Z_{pzt}}{(Z_{air}+Z_{pzt})^2} \approx 5.03 \times 10^{-5} \quad (11)$$

This indicates that ≈ 99.99% of incident energy is reflected. Theoretically, a matching layer with impedance Zmatch = ZairZpzt ≈ 0.11 MRayl allows 100% transmission at the design frequency.

C. Practical Implementation Strategies for Matching Layers

Implementing a matching layer for human speech frequencies (1 kHz) presents unique challenges compared to ultrasonic applications. We propose three concrete strategies for future fabrication:

1. Material Engineering (Syntactic Foams): Standard polymers are too dense (Z > 1.5 MRayl). To achieve the target Zmatch ≈ 0.11 MRayl, we propose using **Syntactic Foams**—a composite of hollow glass microspheres embedded in a flexible epoxy matrix. By controlling the volume fraction of the microspheres, the density (ρ) and sound speed (c) can be tuned to hit the exact impedance target.
2. Acoustic Metamaterials for Sub-wavelength Thickness: A classical λ/4 matching layer at 1 kHz would be impracticably thick (> 8 cm). To maintain the compact form factor of IoT devices, **Acoustic Metamaterials (AMMs)** offer a solution. By 3D-printing labyrinthine or space-coiling structures on the harvester's face, the effective path length of sound waves is extended, artificially lowering the sound speed. This allows a thin layer (< 5 mm) to behave like a macroscopic quarter-wave transformer.
3. Broadband Gradient Layers: Since speech is broadband (500-3000 Hz), a single-layer match is insufficient. Future work will investigate **Gradient Index (GRIN)** layers, where the acoustic impedance changes continuously from Zair to Zpzt (e.g., using multiple layers of aerogel with varying densities). This structure acts as an acoustic funnel, minimizing reflection over a wide bandwidth rather than a single resonant frequency.

D. Feasibility for IoT Applications

Even with the current unoptimized efficiency, the system fits the" Sleep-and-Listen" profile:

1. Current State: Suitable for triggering wake-up circuits or logging rare events.
2. Future State (with Metamaterials): Could power continuous transmission for Low-Power Wide-Area Networks (LPWAN).

CONCLUSION

This study presented a high-fidelity modeling and validation approach for Linear Piezo Motor-based energy harvesting. While the reported efficiency (0.42%) is typical for unoptimized acoustic interfaces, the substantial novelty of this work resides in leveraging the LPM's broadband capability and the real-time simulation of non-deterministic, human speech signals. By incorporating SPL-to-Stress physics and leakage currents, we demonstrated that the system can deliver functional energy in near-field speech scenarios. The experimental results, expanding upon both voltage and real power measurements at the ISO standard 1 kHz reference, confirmed the model's accuracy (error < 6% in the linear region). The study concludes that while LPMs offer a robust, broadband alternative to fragile cantilever beams, their utility is maximized in intermittent, low-duty-cycle IoT applications, provided that acoustic impedance matching techniques are employed in future iterations to enhance overall transmission efficiency.

References

[1] S. R. Anton and H. A. Sodano," A review of power harvesting from vibration using piezoelectric materials," Smart Mater. Struct., vol. 16, 2007.
[2] Standard ISO 226:2003," Acoustics — Normal equal-loudness-level contours."
[3] A. Erturk," Piezoelectric energy harvesting," Wiley, 2011.
[4] S. Roundy," On the effectiveness of vibration-based energy harvesting," J. Intell. Mater. Syst. Struct., vol. 16, 2005.
[5] S. B. Horowitz, M. Sheplak, L. N. Cattafesta, and T. Nishida," A MEMS acoustic energy harvester," J. Micromech. Microeng., vol. 16, no. 9, pp. S174–S181, 2006.
[6] F. Liu, A. Phipps, S. Horowitz, K. Ngo, L. Cattafesta, T. Nishida, and M. Sheplak," Acoustic energy harvesting using an electromechanical Helmholtz resonator," J. Acoust. Soc. Am., vol. 123, no. 4, pp. 1983–1990, 2008.
[7] B. Li, J. H. You, and Y.-J. Kim," Low frequency acoustic energy harvesting using PZT piezoelectric plates in a straight tube resonator," Smart Mater. Struct., vol. 22, no. 5, 055013, 2013.
[8] M. Yuan, Z. Cao, J. Luo, and X. Chou," Recent developments of acoustic energy harvesting: A review," Micromachines, vol. 10, no. 1, p. 48, 2019.
[9] K. Uchino," Piezoelectric ultrasonic motors: overview," Smart Mater. Struct., vol. 7, no. 3, pp. 273–285, 1998.
[10] T. Sashida and T. Kenjo, An Introduction to Ultrasonic Motors. Oxford, U.K.: Clarendon Press, 1993.
[11] T. Mashimo," Micro ultrasonic linear motor using V-shape transducer," IEEE Trans. Ultrason., Ferroelect., Freq. Control, vol. 62, no. 6, pp. 1190–1195, 2015.
[12] J. Hemsel and J. Wallaschek," Survey of the present state of the art of piezoelectric linear motors," Ultrasonics, vol. 38, no. 1-8, pp. 37–40, 2000.
[13] G. K. Ottman, H. F. Hofmann, A. C. Bhatt, and G. A. Lesieutre," Adaptive piezoelectric energy harvesting circuit for wireless remote power supply," IEEE Trans. Power Electron., vol. 17, no. 5, pp. 669–676, 2002.
[14] E. Lefeuvre, A. Badel, C. Richard, L. Petit, and D. Guyomar," A comparison between several vibration-powered piezoelectric

generators for standalone systems," Sensors Actuators A: Phys., vol. 126, no. 2, pp. 405–416, 2006.
[15] Y. K. Ramadass and A. P. Chandrakasan," An efficient piezoelectric energy harvesting interface circuit using a bias-flip rectifier technique," IEEE J. Solid-State Circuits, vol. 45, no. 1, pp. 189–204, 2010.
[16] J. Liang and W.-H. Liao," Impedance modeling and analysis for piezoelectric energy harvesting systems," IEEE/ASME Trans. Mechatronics, vol. 17, no. 6, pp. 1145–1157, 2012.
[17] A. Erturk and D. J. Inman," A distributed parameter electromechanical model for cantilevered piezoelectric energy harvesters," J. Vib. Acoust., vol. 130, no. 4, 041002, 2008.
[18] M. A. Halim, H. Cho, and J. Y. Park," Harvesting energy from human motion using a frequency up-converting electromagnetic energy harvester," Int. J. Precis. Eng. Manuf.-Green Tech., vol. 2, no. 1, pp. 61–67, 2015.
[19] S. Sherrit, S. P. Leary, B. P. Dolgin, and Y. Bar-Cohen," Comparison of the Mason and KLM equivalent circuits for piezoelectric resonators in the thickness mode," 2009 IEEE Int. Ultrason. Symp., 1999, pp.
921–926.